

# Confined $p$ -band Bose-Einstein condensates

Fernanda Pinheiro<sup>1,2,\*</sup>, Jani-Petri Martikainen<sup>2,3</sup>, and Jonas Larson<sup>1,4</sup>

<sup>1</sup>*Department of Physics, Stockholm University, SE-106 91 Stockholm, Sweden*

<sup>2</sup>*NORDITA, SE-106 91 Stockholm, Sweden*

<sup>3</sup>*Aalto University, P.O. Box 1510, FI-00076 Aalto, Finland and*

<sup>4</sup>*Institut für Theoretische Physik, Universität zu Köln, Köln, De-50937, Germany*

(Dated: September 6, 2018)

We study bosonic atoms on the  $p$ -band of a two dimensional optical square lattice in the presence of a confining trapping potential. Using a mean-field approach, we show how the anisotropic tunneling for  $p$ -band particles affects the cloud of condensed atoms by characterizing the ground state density and the coherence properties of the atomic states both between sites and atomic flavors. In contrast to the usual results based on the LDA, the atomic density can become anisotropic. This anisotropic effect is especially pronounced in the limit of weak atom-atom interactions and of weak lattice amplitudes, i.e. when the properties of the ground state are mainly driven by the kinetic energies. We also investigate how the trap influences known properties of the non-trapped case. In particular, we focus on the behavior of the anti-ferromagnetic vortex-antivortex order, which for the confined system, is shown to disappear at the edges of the condensed cloud.

PACS numbers: 03.75.Lm, 03.75.Mn

## I. INTRODUCTION

With refined experimental techniques in trapping and cooling, atomic gases have become prime candidates for studies of mesoscopic quantum phenomena [1]. Among different possible experimental configurations [1, 2], systems of cold atoms subjected to optical lattices constitute one of the most active topics of the current research in the field. In the ultracold limit, these setups may serve as *quantum simulators* which can be used to test actual models of condensed matter theories in a precise way [2]. In fact, the degree of experimental control in optical lattice systems is so great, that by tuning the parameters of the lattice the atoms can be moved into the strongly correlated regime, therefore allowing for the study of a variety of phenomena which include quantum phase transitions [3]. Beyond experimental manipulations of the ground state, the versatility of these systems also makes it possible to experimentally prepare certain excited states. In this respect, of particular interest are the states of bosons restricted to the first excited energy bands of the lattice, the so called  $p$ -band bosons.

Qualitatively, the physics of  $p$ -band bosons is considerably different from the well studied systems where the bosons are only restricted to the lowest band ( $s$ -band bosons). The reason for this can be intuitively understood from the isotropic square and cubic lattices, where the symmetry of the lattice implies a double (square lattice) and triple (cubic lattice) degeneracy [4, 5] on the  $p$ -band. In solid state systems such degeneracies could be removed via Jahn-Teller effects, but since here the lattice is imposed from the outside, the degeneracy is robust. This degeneracy motivates the description of the atomic states in terms of orbitals related to the corre-

sponding localized Wannier functions, characterized by a node in each of the spatial directions. In the direction of the node, the Wannier functions are also broader and since this directly influences the ease of tunneling between sites, it directly affects the dynamical properties of the system. Since the properties of the tunneling of  $p$ -band bosons are dramatically altered from the ones on the  $s$ -band, a rich variety of novel quantum phases [6–9] can appear. When interactions are taken into account, it has also been argued that in the limit of very strong atom-atom interactions, atomic population can move to higher energy bands, affecting thus the expected ground state properties of ultracold atoms in optical lattices [10–15]. The broadening of the onsite wave-functions, for example, was experimentally verified via microwave spectroscopy [16]. In addition, signatures of (strong) interaction induced higher bands physics could also be seen in non-equilibrium configurations, through the mapping of collapse-revivals structures in the atomic density [17] (see also Ref. [18]). Surprising effects are also present in the limit of weak interactions. In fact, it was recently observed [19, 20] that due to unusual dispersions, the physics of  $p$ -band bosons appears responsible for unconventional condensation, where non-zero momentum states [21] are occupied. We should point out, however, that even though experiments concerning  $p$ -band physics have been restricted to one dimensional, square or cubic lattices [19, 20, 22, 23], several theoretical predictions have been made for other lattice configurations [24].

In experiments, optical lattice systems are generally subjected to an external confining trap. Although it is known that even for  $s$ -band bosons, the presence of the trap can add important features to the physics of the system [25], all the aforementioned theoretical studies of  $p$ -band bosonic systems neglect effects originating from the confining trap potential. Thus, it is important to study how the inclusion of a trap affects the  $p$ -band

---

\* fep@fysik.su.se

physics. For example, in the case of a two dimensional (2D) lattice it is characteristic of  $p$ -band bosons to have tunneling coefficients with different amplitudes in different directions. In the non-trapped case, this property of anisotropic tunneling together with the properties of homogeneous density distributions yields a corresponding ground state which has an anti-ferromagnetic order with vortex/anti-vortex states on every second site (also known as the state of staggered orbital angular momentum) [5, 9]. In trapped systems, however, the property of anisotropic tunneling necessarily introduces density inhomogeneities which break the population balance between different possible atomic states (here corresponding to the two possible orbitals of the 2D lattice). This also gives rise to physics beyond the one captured by using the local density approximation (LDA). The fate of the anti-ferromagnetic order in the presence of the trap is then unclear.

In this paper we study this issue and address also other effects and properties which arise when  $p$ -band bosons are confined by an external potential. We mostly restrict the analysis to 2D, but discuss how the obtained results generalize to 3D. The analysis is based on the ideal gas theory and a mean-field approach, where we assume the system to be deep in the region of the superfluid phase. We start by presenting the theoretical framework and follow with the study of the ideal system at finite temperatures, where the critical temperature for condensation in a non-interacting  $p$ -band bosonic gas is calculated. We then show that for a symmetric square lattice, the zero temperature order parameter of the condensed ground state is complex also in the presence of a trap, but the vortex/anti-vortex structure can be lost. In particular, the ground state for the  $p$ -band atomic densities of the two flavors are shown to be different except for when the system is driven into the Thomas-Fermi (TF) regime in which case we can neglect effects stemming from the kinetic tunneling energy. We complete the study with an analysis of the zero temperature properties of an asymmetric lattice. We find that due to splitting of the  $p$ -band degeneracy, the ground state properties may be sensitive to small changes in the two lattice amplitudes.

It is important to point out that our analysis is carried out when influence from other bands have been omitted. The validity of this assumption is specially tested in the harmonic approximation, where two  $p$ -band atoms become degenerate with one  $s$ - and one  $d$ - atom. In fact, due to a 'reduced final density of states for scattering processes' [23], these decays can be significantly suppressed [5] and the lifetimes of the atoms in  $p$ - orbitals become 1-2 order of magnitude larger than typical tunneling times. In addition, outside the harmonic approximation as the case considered throughout this paper, the actual anharmonicity of the lattice breaks the  $(p + p \rightarrow s + d)$  degeneracy for almost all quasi momenta, suppressing further such loss processes.

## II. DERIVATION OF THE EFFECTIVE MODEL HAMILTONIAN

### A. Hamiltonian for $p$ -band bosons

In terms of the field operators  $\hat{\Psi}(\vec{r}')$ , the dynamics of the weakly interacting Bose gas can be described by the Hamiltonian

$$H = \int d\vec{r}' \left\{ \hat{\Psi}^\dagger(\vec{r}') \left[ -\frac{\hbar^2 \nabla^2}{2m} + V(\vec{r}') \right] \hat{\Psi}(\vec{r}') + \frac{\tilde{U}_0}{2} \hat{\Psi}^\dagger(\vec{r}') \hat{\Psi}^\dagger(\vec{r}') \hat{\Psi}(\vec{r}') \hat{\Psi}(\vec{r}') \right\}, \quad (1)$$

where  $m$  corresponds to the mass of the particles,  $\tilde{U}_0$  to the strength of the interparticle interaction, and  $V(\vec{r}')$  accounts for the effects of external potentials acting on the system. The field operators  $\hat{\Psi}(\vec{r}')$  and  $\hat{\Psi}^\dagger(\vec{r}')$  annihilate and create a particle at position  $\vec{r}'$  respectively, and obey the standard boson commutation relation  $[\hat{\Psi}(\vec{r}''), \hat{\Psi}^\dagger(\vec{r}')] = \delta(\vec{r}'' - \vec{r}')$ . In this work we consider a trapped system in 2D with  $V(\vec{r}') = V_{latt}(\vec{r}') + V_{trap}(\vec{r}')$ , where the optical lattice potential

$$V_{latt}(\vec{r}') = \tilde{V}_x \sin^2(kx') + \tilde{V}_y \sin^2(ky') \quad (2)$$

has amplitudes and wave vector given, respectively, by  $\tilde{V}_\alpha$ ,  $\alpha \in \{x, y\}$ , and  $k = 2\pi/\lambda$ , with  $\lambda$  being the wave length of the applied lasers, and where

$$V_{trap}(\vec{r}') = \frac{m\tilde{\omega}^2}{2} (x'^2 + y'^2) \quad (3)$$

describes the action of an overall slowly varying harmonic trap with frequency  $\tilde{\omega}$ .

The common practice in the study of many-body systems subjected to periodic potentials consists in the expansion of the many-body Hamiltonian in terms of a suitable basis, generally constructed from its corresponding non-interacting part. In fact, the invariance under discrete translations of the lattice implies conservation of quasi-momentum and an energy spectrum having a band structure, which therefore immediately suggest the use of Bloch functions. Here, however, the presence of the trap breaks translational invariance and implies a finite size for the system, consequently destroying the symmetries that rigorously justify theoretical treatment in these terms. On the other hand, the smoothness of the potential implies that its characteristic length scale fulfills the condition  $l_{trap} = \sqrt{\hbar/m\tilde{\omega}} \gg \lambda/2$ , and thus we can implement the effects of the trap in each site, by only shifting the onsite energies and assuming that the onsite orbitals remain the same in the absence of a trap. This means that locally the system is still effectively periodic, and that a satisfactory approximation can be obtained from the traditional framework.

Before carrying out the expansion of the field operators we define dimensionless parameters by taking the

recoil energy  $E_r = \hbar^2 k^2 / 2m$  as the energy scale (i.e. all energies are scaled by this quantity) and the inverse wave vector as the typical length scale  $l = \lambda / 2\pi$ , which produces a dimensionless trap frequency given by  $\omega = \sqrt{2}m\tilde{\omega} / \hbar k^2$ . In these terms, the trapping potential becomes  $V(\vec{r}) = \omega^2 (x^2 + y^2) / 2$ , with  $x = kx'$  and  $y = ky'$  the dimensionless positions. From now on, we assume these units in all the derivations so that resulting equations are dimensionless. As a first step, we construct the bosonic operators  $\hat{b}_{\nu\mathbf{q}}$  and  $\hat{b}_{\nu\mathbf{q}}^\dagger$  which create and annihilate, respectively, one particle delocalized in the Bloch state  $\phi_{\nu\mathbf{q}}(\vec{r})$  of quasi-momentum  $\mathbf{q} = (q_x, q_y)$  in the  $\nu$ -th energy band, and use it to write

$$\begin{aligned}\hat{\Psi}^\dagger(\vec{r}) &= \sum_{\nu\mathbf{q}} \phi_{\nu\mathbf{q}}^*(\vec{r}) \hat{b}_{\nu\mathbf{q}}^\dagger, \\ \hat{\Psi}(\vec{r}) &= \sum_{\nu\mathbf{q}} \phi_{\nu\mathbf{q}}(\vec{r}) \hat{b}_{\nu\mathbf{q}},\end{aligned}\tag{4}$$

where the  $\nu$ -sum runs over all energy bands, and the  $\mathbf{q}$ -sum is over the first Brillouin zone. We also use the above expressions to construct the site-localized Wannier functions, where the operators read

$$\begin{aligned}\hat{\Psi}^\dagger(\vec{r}) &= \sum_{\nu\mathbf{j}} w_{\nu\mathbf{R}_j}^*(\vec{r}) \hat{a}_{\nu\mathbf{j}}^\dagger, \\ \hat{\Psi}(\vec{r}) &= \sum_{\nu\mathbf{j}} w_{\nu\mathbf{R}_j}(\vec{r}) \hat{a}_{\nu\mathbf{j}}.\end{aligned}\tag{5}$$

Here,  $\mathbf{R}_j = (x_j, y_j) = (\pi j_x, \pi j_y)$  labels the coordinates of the  $j$ 'th site of the lattice ( $\mathbf{j} = (j_x, j_y)$ ,  $j_x, j_y \in \mathcal{N}$ ), and  $\hat{a}_{\nu\mathbf{j}}$  ( $\hat{a}_{\nu\mathbf{j}}^\dagger$ ) annihilate (create) a particle in the Wannier state  $w_{\nu\mathbf{R}_j}(\vec{r})$ . For completeness, the relation between Wannier and Bloch functions is given by

$$w_{\nu\mathbf{R}_j}(\vec{r}) = \sum_{\mathbf{q}} e^{-i\mathbf{q}\cdot\mathbf{R}_j} \phi_{\nu\mathbf{q}}(\vec{r}).\tag{6}$$

As a second step in deriving an effective model described by the Hamiltonian of Eq. (1), we choose the expansion of the many-body Hamiltonian in terms of (5) and introduce some approximations. Our option for this picture is justified by the fact that while considerably simpler for the practical implementations, the use of Wannier basis together with the tight-binding approximation can still provide a good description as long as the lattice is deep enough [26]. In addition to restricting the hopping to nearest-neighbors (tight-binding), we truncate the expansion of the field operators to include only the  $p$ -bands.

As the last step of our derivation, we clarify the used terminology. For a square lattice, the two  $p$ -band Wannier functions at each site  $\mathbf{j}$  are characterized by a node along either the  $x$ - or  $y$ - directions. Therefore we call atoms with orbital wavefunctions,  $w_{x\mathbf{j}}(\vec{r})$  and  $w_{y\mathbf{j}}(\vec{r})$ , respectively as  $x$ - and  $y$ -flavors [5], and for completeness

we give their explicit expressions

$$\begin{aligned}w_{x\mathbf{j}}(\vec{r}) &= w_{2j_x}(x)w_{1j_y}(y), \\ w_{y\mathbf{j}}(\vec{r}) &= w_{1j_x}(x)w_{2j_y}(y).\end{aligned}\tag{7}$$

From this, the nature of the node-structure becomes clear. It is a direct consequence of the nodal structure of the Wannier functions  $w_{2j}(x)$  and  $w_{1j}(x)$ . An  $x$ -flavor (or equivalently  $p_x$ -orbital) atom, thus, not only has a wavefunction with a node along the  $x$ -direction, but also a broader distribution along  $x$ . Accordingly, the opposite is true for atoms in the  $y$ -flavor. This property directly affects the tunneling properties of the atoms in this system.

Putting everything together, we can write down the resulting many-body Hamiltonian

$$H = H_0 + H_{nn} + H_{FD},\tag{8}$$

with the ideal part given by

$$H_0 = - \sum_{\alpha,\beta} \sum_{\langle\mathbf{ij}\rangle_\alpha} t_{\alpha\beta} \hat{a}_{\beta\mathbf{i}}^\dagger \hat{a}_{\beta\mathbf{j}} + \sum_{\alpha} \sum_{\mathbf{j}} V_{trap}(\mathbf{R}_j) \hat{n}_{\alpha\mathbf{j}},\tag{9}$$

where  $\sum_{\langle\mathbf{ij}\rangle_\alpha}$  refers to the sum over nearest neighbors in the direction  $\alpha$  ( $\alpha, \beta = x, y$ ) and  $\hat{n}_{\alpha\mathbf{j}} = \hat{a}_{\alpha\mathbf{j}}^\dagger \hat{a}_{\alpha\mathbf{j}}$  is the atom number operator; and where the interaction terms

$$H_{nn} = \sum_{\alpha} \sum_{\mathbf{j}} \frac{U_{\alpha\alpha}}{2} \hat{n}_{\alpha\mathbf{j}} (\hat{n}_{\alpha\mathbf{j}} - 1) + \sum_{\alpha\beta, \alpha \neq \beta} \sum_{\mathbf{j}} U_{\alpha\beta} \hat{n}_{\alpha\mathbf{j}} \hat{n}_{\beta\mathbf{j}},\tag{10}$$

and

$$\begin{aligned}H_{FD} &= \sum_{\alpha\beta, \alpha \neq \beta} \sum_{\mathbf{j}} \frac{U_{\alpha\beta}}{2} \left( \hat{a}_{\alpha\mathbf{j}}^\dagger \hat{a}_{\alpha\mathbf{j}}^\dagger \hat{a}_{\beta\mathbf{j}} \hat{a}_{\beta\mathbf{j}} \right. \\ &\quad \left. + \hat{a}_{\beta\mathbf{j}}^\dagger \hat{a}_{\beta\mathbf{j}}^\dagger \hat{a}_{\alpha\mathbf{j}} \hat{a}_{\alpha\mathbf{j}} \right),\end{aligned}\tag{11}$$

account, respectively, for contribution of density-density and interflavor conversion interactions. The expression for the interaction parameters is given by

$$U_{\alpha\beta} = U_0 \int d\vec{r} |w_{\alpha\mathbf{j}}(\vec{r})|^2 |w_{\beta\mathbf{j}}(\vec{r})|^2,\tag{12}$$

and for the tunneling coefficients by

$$t_{\alpha\beta} = - \int d\vec{r} w_{\alpha\mathbf{j}}^*(\vec{r}) [-\nabla^2 + V(\vec{r})] w_{\alpha\mathbf{j}+\mathbf{1}_\beta}(\vec{r}),\tag{13}$$

where by  $\mathbf{j} + \mathbf{1}_\beta$  we indicate the neighboring site of  $\mathbf{j}$  in the direction  $\beta$ , and  $U_0 = \tilde{U}_0 l^3 / E_r$ ,  $V_\beta = \tilde{V}_\beta / E_r$  are the dimensionless interparticle strength and lattice amplitudes, respectively. From here, after substitution of the Wannier functions (7) into the above equation (13), it is straightforward to see that contributions for the tunneling coefficient in the direction perpendicular to the

node depend uniquely from Wannier functions of the first band (i.e.  $\nu = 1$ ), while in the direction of the node it solely depends on the second band Wannier functions ( $\nu = 2$ ). As a consequence, an  $x$ -flavor atom has larger probability of tunneling in the  $x$ -direction than in the  $y$ -direction, while the opposite also holds for a  $y$ -flavor atom. We continue discussions regarding the effects of this anisotropic tunneling in Sec. III. Also, before proceeding with the mean-field derivations, we make a brief comment on the symmetries of the Hamiltonian (8). As pointed out in Ref. [5], this Hamiltonian has an associated  $Z_2$  symmetry, related to the parity of atomic flavors: since atom scattering processes occur in pairs, the number of  $x$ -flavor atoms  $N_x$  and  $y$ -flavor atoms  $N_y$  are preserved modulo 2. Isotropic lattices support, in addition, a symmetry corresponding to swapping of atomic flavors  $x \leftrightarrow y$ . We will also discuss how this property implies a double degeneracy of the ground state for the infinite system.

### B. Mean-field Hamiltonian

Except when otherwise stated, all our results follow from analysis of the 2D lattice. We assume the condensate confined in the transverse  $z$ -direction, and thus at each lattice site the system could either be purely two-dimensional or form condensed tubes with typically a few hundred of atoms [27]. In either configuration, a mean-field treatment is expected to give a reliable picture of the relevant physics [9].

At a mean-field level, the operators  $\hat{a}_{\alpha\mathbf{j}}$  are replaced by the complex numbers  $\psi_{\alpha\mathbf{j}}$ . This approximation is equivalent to assigning a coherent state at each site,  $|\Psi\rangle = \bigotimes_{\mathbf{j}} |\psi\rangle_{\mathbf{j}} = \bigotimes_{\mathbf{j}} |\psi_{x\mathbf{j}}, \psi_{y\mathbf{j}}\rangle_{\mathbf{j}}$  such that  $\hat{a}_{\alpha\mathbf{j}}|\Psi\rangle = \psi_{\alpha\mathbf{j}}|\Psi\rangle$ . In terms of the Fock basis, the single site many-body wavefunction reads

$$|\psi\rangle_{\mathbf{j}} = \exp\left(-\frac{|\psi_{x\mathbf{j}}|^2 + |\psi_{y\mathbf{j}}|^2}{2}\right) \sum_{n_x, n_y} \frac{\psi_{x\mathbf{j}}^{n_x} \psi_{y\mathbf{j}}^{n_y}}{\sqrt{n_x! n_y!}} |\mathbf{n}\rangle_{\mathbf{j}}, \quad (14)$$

where  $|\mathbf{n}\rangle_{\mathbf{j}} = |n_x, n_y\rangle_{\mathbf{j}}$  represents the state of  $n_x$   $x$ -flavor atoms and  $n_y$   $y$ -flavor atoms at site  $\mathbf{j}$ . Moreover, in this language the onsite order parameter of site  $\mathbf{j}$  and flavor  $\alpha$  reads  $\psi_{\alpha\mathbf{j}} = \langle \Psi | \hat{a}_{\alpha\mathbf{j}} | \Psi \rangle$ .

With the coherent state ansatz we can obtain the equations of motion for the order parameter  $\psi_{\alpha\mathbf{j}}$  from the Euler-Lagrange equations

$$\frac{\partial L}{\partial \psi_{\alpha\mathbf{j}}^*} - \frac{d}{dt} \left( \frac{\partial L}{\partial \dot{\psi}_{\alpha\mathbf{j}}^*} \right) = 0, \quad (15)$$

where the Lagrangian is given by

$$L = \sum_{\alpha} \sum_{\mathbf{j}} i \frac{1}{2} \left[ \psi_{\alpha\mathbf{j}}^* \frac{d}{dt} \psi_{\alpha\mathbf{j}} - \psi_{\alpha\mathbf{j}} \frac{d}{dt} \psi_{\alpha\mathbf{j}}^* \right] - H_{MF}, \quad (16)$$

with the mean-field Hamiltonian

$$\begin{aligned} H_{MF} = & - \sum_{\alpha, \beta} \sum_{\langle \mathbf{i}\mathbf{j} \rangle_{\alpha}} t_{\alpha\beta} \psi_{\alpha\mathbf{i}}^* \psi_{\alpha\mathbf{j}} + \sum_{\alpha} \sum_{\mathbf{j}} \frac{U_{\alpha\alpha}}{2} n_{\alpha\mathbf{j}} n_{\alpha\mathbf{j}} \\ & + \sum_{\alpha} \sum_{\mathbf{j}} \frac{\omega^2}{2} (x_{\mathbf{j}}^2 + y_{\mathbf{j}}^2) n_{\alpha\mathbf{j}} \\ & + \sum_{\alpha\beta, \alpha \neq \beta} \sum_{\mathbf{j}} U_{\alpha\beta} n_{\alpha\mathbf{j}} n_{\beta\mathbf{j}} + \sum_{\alpha\beta, \alpha \neq \beta} \sum_{\mathbf{j}} \frac{U_{\alpha\beta}}{2} \\ & \times \left( \psi_{\alpha\mathbf{j}}^* \psi_{\alpha\mathbf{j}} \psi_{\beta\mathbf{j}} \psi_{\beta\mathbf{j}} + \psi_{\beta\mathbf{j}}^* \psi_{\beta\mathbf{j}} \psi_{\alpha\mathbf{j}} \psi_{\alpha\mathbf{j}} \right), \end{aligned} \quad (17)$$

and where the Hamiltonian (8) has been normally ordered prior to calculation of the coherent state expectation value. Here the density of the flavor  $\alpha$  is given by  $n_{\alpha\mathbf{j}} = |\psi_{\alpha\mathbf{j}}|^2$  and normalization was imposed in the whole lattice as

$$N = N_x + N_y = \sum_{\mathbf{j}} |\psi_{x\mathbf{j}}|^2 + \sum_{\mathbf{j}} |\psi_{y\mathbf{j}}|^2, \quad (18)$$

with  $N$  accounting for the total number of atoms.

The Euler-Lagrange equations then correspond to a set of coupled Gross-Pitaevskii equations, one for each atomic  $\alpha$ -flavor at each site  $\mathbf{j}$ :

$$\begin{aligned} i \frac{\partial \psi_{x\mathbf{j}}}{\partial t} = & - \sum_{\beta \in \{x, y\}} t_{x\beta} \left( \psi_{x\mathbf{j}+\mathbf{1}_{\beta}} - 2\psi_{x\mathbf{i}} + \psi_{x\mathbf{j}-\mathbf{1}_{\beta}} \right) \\ & + \frac{\omega^2}{2} (x_{\mathbf{j}}^2 + y_{\mathbf{j}}^2) \psi_{x\mathbf{j}} \\ & + (U_{xx} |\psi_{x\mathbf{j}}|^2 + 2U_{xy} |\psi_{y\mathbf{j}}|^2) \psi_{x\mathbf{j}} \\ & + (U_{xy} + U_{yx}) \psi_{y\mathbf{j}}^2 \psi_{x\mathbf{j}}^* \\ i \frac{\partial \psi_{y\mathbf{j}}}{\partial t} = & - \sum_{\beta \in \{x, y\}} t_{y\beta} \left( \psi_{y\mathbf{j}+\mathbf{1}_{\beta}} - 2\psi_{y\mathbf{i}} + \psi_{y\mathbf{j}-\mathbf{1}_{\beta}} \right) \\ & + \frac{\omega^2}{2} (x_{\mathbf{j}}^2 + y_{\mathbf{j}}^2) \psi_{y\mathbf{j}} \\ & + (U_{yy} |\psi_{y\mathbf{j}}|^2 + 2U_{yx} |\psi_{x\mathbf{j}}|^2) \psi_{y\mathbf{j}} \\ & + (U_{yx} + U_{xy}) \psi_{x\mathbf{j}}^2 \psi_{y\mathbf{j}}^*. \end{aligned} \quad (19)$$

Like all other parameters and variables, time  $t$  is a dimensionless quantity. Note also that we take all the parameters entering the above equations from numerically obtained Wannier overlap integrals according to Eqs. (12) and (13), and consequently no harmonic approximation is imposed. This avoids some qualitatively wrong conclusions which can occur with the latter assumption [11].

### III. IDEAL GAS

#### A. Ground state properties

Let us first investigate some features of the system in the non-interacting case, where the free mean-field Hamiltonian is given by

$$H_{MF}^{(0)} = - \sum_{\alpha, \beta} \sum_{\langle \mathbf{i} \mathbf{j} \rangle_{\alpha}} t_{\alpha\beta} \psi_{\alpha\mathbf{i}}^* \psi_{\alpha\mathbf{j}} + \sum_{\alpha} \sum_{\mathbf{j}} \frac{\omega^2}{2} (x_{\mathbf{j}}^2 + y_{\mathbf{j}}^2) n_{\alpha\mathbf{j}}. \quad (20)$$

In the absence of interflavor interactions, interflavor onsite coherence is not established. However, within each flavor it is the tunneling which determines how the phases of neighboring sites are related to each other. We thus characterize these properties for the ground-state by minimizing (20). To this end, the expression for the onsite order parameters is taken as  $\psi_{\alpha\mathbf{j}} = |\psi_{\alpha\mathbf{j}}| e^{i\phi_{\alpha\mathbf{j}}}$ , and by noticing that  $t_{xx}, t_{yy} < 0$  and  $t_{xy}, t_{yx} > 0$  we obtain a striped order in the phase of each flavor. More explicitly, the phase of the  $x$ -flavor order parameter can be expressed as  $\phi_{x\mathbf{j}} = \phi_x(j_x, j_y) = \pi \times \text{mod}(j_x, 2)$ . This means that neighboring sites will always keep the same phase in the direction perpendicular of the node, while in the parallel direction the phase difference will be  $\pi$ .

The discrete model (20) can in principle be solved analytically by noticing that the Hamiltonian matrix has the same structure as the one of the Mathieu equation expanded in momentum eigenstates [28]. The solutions is not very instructive as it is determined from the Fourier expansion of the Mathieu functions, i.e. by the transformation matrix between quasi- and real momentum. A simple physical picture of the influence of the trap in the discrete model is instead better analyzed in the continuum limit where the analytical solutions can be given in closed forms. Here it is convenient to work with the order parameters without phase modulation. We thus impose the correct phase imprint responsible for rendering the striped order into the wavefunction ansatz. Under these circumstances, the phase factors can be absorbed into the redefinition of the tunneling coefficient,  $t_{\alpha\alpha} \rightarrow -t_{\alpha\alpha}$ . In addition, the continuum limit consists in  $\psi_{\alpha\mathbf{j}} \rightarrow \psi_{\alpha}(x, y)$ , and the kinetic energy transforms as

$$\psi_{\alpha\mathbf{j}+1_{\beta}} - 2\psi_{\alpha\mathbf{i}} + \psi_{\alpha\mathbf{j}-1_{\beta}} \longrightarrow \frac{\partial^2}{\partial \beta^2} \psi_{\alpha}(\alpha, \beta). \quad (21)$$

With this approximation, we obtain the following contin-

uum equations

$$i \frac{\partial}{\partial t} \psi_x(x, y) = \left[ -|t_{xx}| \frac{\partial^2}{\partial x^2} - |t_{xy}| \frac{\partial^2}{\partial y^2} + \frac{\omega^2}{2} (x^2 + y^2) \right] \psi_x(x, y), \quad (22)$$

$$i \frac{\partial}{\partial t} \psi_y(x, y) = \left[ -|t_{yy}| \frac{\partial^2}{\partial y^2} - |t_{yx}| \frac{\partial^2}{\partial x^2} + \frac{\omega^2}{2} (x^2 + y^2) \right] \psi_y(x, y),$$

where  $x$  and  $y$  are dimensionless. By introducing the effective mass  $m_{\alpha\beta} = |t_{\alpha\beta}|^{-1}/2$  and parallel and transverse frequencies

$$\omega_{\parallel} = \omega \sqrt{2|t_{\alpha\beta}|}, \quad \alpha \neq \beta, \quad (23)$$

$$\omega_{\perp} = \omega \sqrt{2|t_{\alpha\beta}|}, \quad \alpha = \beta,$$

Eq. (22) can be written as

$$i \frac{\partial}{\partial t} \psi_x(x, y) = \left[ \frac{p_x^2}{2m_{xx}} + \frac{p_y^2}{2m_{xy}} + \frac{m_{xx}\omega_{\parallel}^2}{2} x^2 + \frac{m_{xy}\omega_{\perp}^2}{2} y^2 \right] \psi_x(x, y), \quad (24)$$

with a similar equation for the  $y$ -flavor. We find, therefore, that the continuum approximation reduces the system to two 2D anisotropic harmonic oscillators. It is important to stress though, that in order to derive Eq. (24), the striped order must be correctly implemented. If the phase modulation is not considered before imposition of the continuum approximation, the resulting Hamiltonian is not bounded from below, and since the lattice naturally introduces a momentum cut-off  $\Lambda = \pi/\lambda$  at the edges of the Brillouin zone, it is a property not present in the discrete model. The initial phase imprint is thus a tool to circumvent this problem, where the overall effect of the procedure translates into inversion of the  $p$ -band and shifting of its minimum to the center of the Brillouin zone.

In the continuum model, the anisotropy arising from the different tunneling elements  $t_{xx}$  and  $t_{xy}$  is directly reflected in the direction-dependence of  $m_{\alpha\beta}$  and  $\omega_{\alpha\beta}$ . Therefore, it follows from this anisotropy that the continuum Gaussian ground state will have different widths in the two directions  $x$  and  $y$ . We use this fact to define the anisotropy parameter

$$S_x = \sqrt{\frac{(\Delta_x x)^2}{(\Delta_x y)^2}}, \quad (25)$$

with equivalent expression to the  $y$ -flavor, and where  $(\Delta_\alpha \beta)^2 = \langle \beta^2 \rangle_\alpha - \langle \beta \rangle_\alpha^2$  and  $\langle \dots \rangle_\alpha$  represents the expectation value taken with respect to  $\psi_\alpha(x, y)$ . For symmetry reasons  $S_x S_y = 1$  must hold, and thus we call the  $x$ -flavor anisotropy parameter simply by  $S$ . This definition is general and applies to both the discrete as well as for the continuum limit. It can be used to derive an explicit expression for the latter case

$$S_{con} = \left( \frac{|t_{xx}|}{|t_{xy}|} \right)^{1/4} = \left( \frac{\omega_{\parallel}}{\omega_{\perp}} \right)^{1/2}, \quad (26)$$

which as expected, predicts  $S = 1$  for isotropic systems (i.e., where both directions have the same tunneling strengths). However, generally  $S \neq 1$ , and therefore it reveals the existence of narrowing in the flavor density along one of the directions. This anisotropy is a consequence of the direction-dependence of the tunneling  $t_{\alpha\beta}$  and is a result beyond the LDA. Note furthermore that when atom-atom interaction has been neglected,  $N_x$  and  $N_y$  are preserved quantities and the actual ground state of the system will be determined from the preparation process. For non-zero atom-atom interaction,  $N_x$  and  $N_y$  are no longer independently preserved due to the term (11) and the interaction energy is minimized with  $N_x = N_y$  as will be seen in the next section. Now we continue with further discussions upon validity and applicability of the continuum approximation.

## B. Ideal gas at finite temperatures

For the ideal gas system, represented by the Hamiltonian (20), it is rather straightforward to calculate finite temperature effects, either from direct numerical diagonalization or using the analytical solutions obtained from Fourier expansions of Mathieu functions. Due to discretization of (20), the eigenstates in the harmonic trap are not the same as the usual eigenstates of the harmonic oscillator. Since implications of this for the thermodynamics of an ideal gas are not clear, we numerically solve the discrete 2D and also 3D Schrödinger equations for the eigenstates, and use these as a basis to study Bose-Einstein condensation on the  $p$ -band in the presence of a trap.

In the continuum limit described by Eq. (22), the critical temperature for the Bose-Einstein condensation in the harmonic trap is well known [29] and given by

$$T_{c0}^{(2D)} = \omega_{eff}^{(2D)} \sqrt{6N/\pi^2} \quad (27)$$

in 2D and in 3D by

$$T_{c0}^{(3D)} = \omega_{eff}^{(3D)} (N/\zeta(3))^{1/3}, \quad (28)$$

with  $\zeta(3) \approx 1.20206$ , and where the trapping frequencies are defined as averages of the effective frequencies (23) as

$$\omega_{eff}^{(2D)} = 4\omega \sqrt{|t_{xx}| |t_{xy}|} \quad (29)$$

and

$$\omega_{eff}^{(3D)} = 4\omega (|t_{xx}| |t_{xy}|^2)^{1/3}. \quad (30)$$

For bosonic gases, the number  $N_T$  of thermal (non-condensed) atoms follows from

$$N_T = \sum_{n \neq 0} \frac{1}{\exp(\beta(E_n - \mu)) - 1}, \quad (31)$$

where  $\beta = E_r/k_B T$  is the inverse (dimensionless) temperature and  $\mu$  is the chemical potential. Together with the eigenenergies  $E_n$  obtained by solving the Schrödinger equation, this can be used to compute the critical temperature for condensation in our lattice model. Notice however, that while below the critical temperature the chemical potential  $\mu$  is equal to the ground state energy, at higher temperatures it must be determined by fixing the total atom number to  $N$ .

We compare the predictions for the critical temperature of the continuum and lattice models in Fig. 1. As is seen, the general result in both the 2D and 3D systems, consists in a somewhat lower critical temperature for very small atom numbers, but substantially larger critical temperature for high atom numbers. Such difference is due to different density of states between the lattice and the continuum models.

In a trap, the transition to the condensed state is typically associated with pronounced changes in the atomic density distribution. A broad thermal distribution above the critical temperature acquires a bimodal structure as a density peak appears in the center corresponding to the macroscopic occupation of the condensate ground state. Also, as already discussed in the previous subsection, in the case of trapped  $p$ -band atoms the anisotropy is a new feature appearing in the density distribution. Above the critical temperature  $T_c$ , the density distribution has the same width in  $x$ - and  $y$ -directions, but below  $T_c$  the condensate density distribution shares the properties of the ground state, which is anisotropic due to different tunneling strengths in different directions. We give an example of this behavior in Fig. 2 by displaying the anisotropy parameter (25) as a function of temperature for 1000 atoms. Furthermore, in Fig. 3 we show the density ( $\psi_n(\mathbf{j})$  are the eigenstate wavefunctions)

$$n_{tot}(\mathbf{j}) = N_0 |\psi_0(\mathbf{j})|^2 + \sum_{n \neq 0} \frac{|\psi_n(\mathbf{j})|^2}{\exp(\beta(E_n - \mu)) - 1} \quad (32)$$

close to  $T_c$  and at  $T = 0$ , demonstrating the appearance of strong anisotropy (for single flavor) at low temperatures.

## IV. INTERACTING GAS

### A. Characterizing the ground state

Until now we have not considered how interactions affect the system's ground state properties. Effects stem-

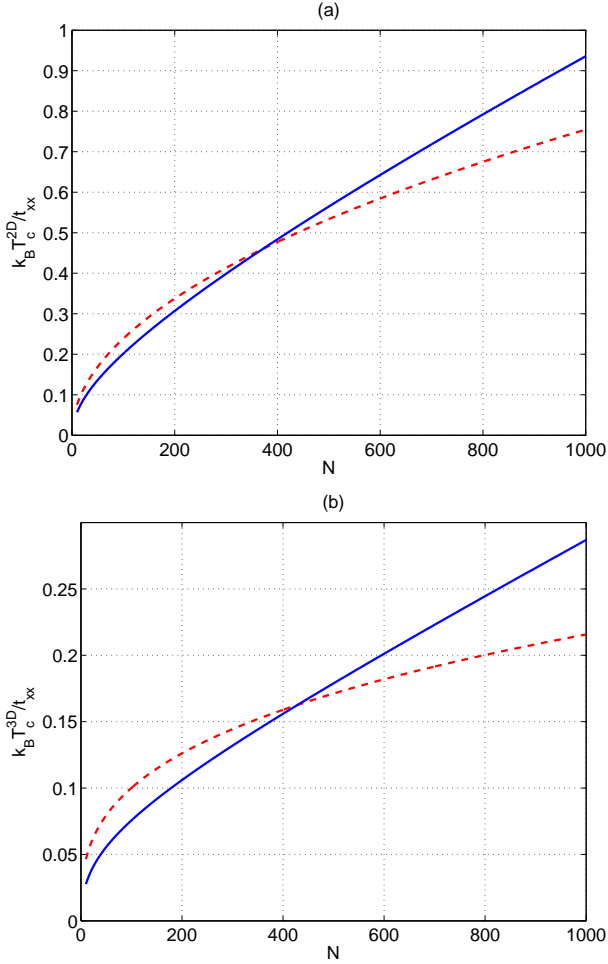


FIG. 1. (Color online) The critical temperature for the Bose-Einstein condensation as a function of atom number  $N$  in (a) 2D system and (b) 3D system. The dashed line shows the result based on approximating the discrete model with a continuum one, and the solid line displays the numerically calculated results of the discrete model. We used the dimensionless trap strength  $\omega^2/2 = 0.001$  and  $|t_{xx}/t_{xy}| = 20.1$  which is our estimate for the ratio of tunneling strengths at  $V_x = V_y = 17$ .

ming from the tunneling part and the corresponding phase ordering imposed in the minimization of the mean-field Hamiltonian were already discussed in Sec. III. We thus complete the characterization of the ground state of the system by repeating this analysis to the interacting part of  $H_{MF}$ . Since neighboring sites are not coupled by the interaction term, it is enough to consider the energy contribution within only one single site. In analogous procedure to the one used in the aforementioned analysis, we substitute the expression  $\psi_{\alpha j} = |\psi_{\alpha j}| e^{i\phi_{\alpha j}}$  for the onsite order parameter of the flavor  $\alpha$ , and the resulting density-density and interflavor conversion parts of the mean-field Hamiltonian follow, respectively, as

$$H_{nn}^{(j)} = \frac{U_{xx}}{2} |\psi_{xj}|^4 + \frac{U_{yy}}{2} |\psi_{yj}|^4 + (U_{xy} + U_{yx}) |\psi_{xj}|^2 |\psi_{yj}|^2 \quad (33)$$

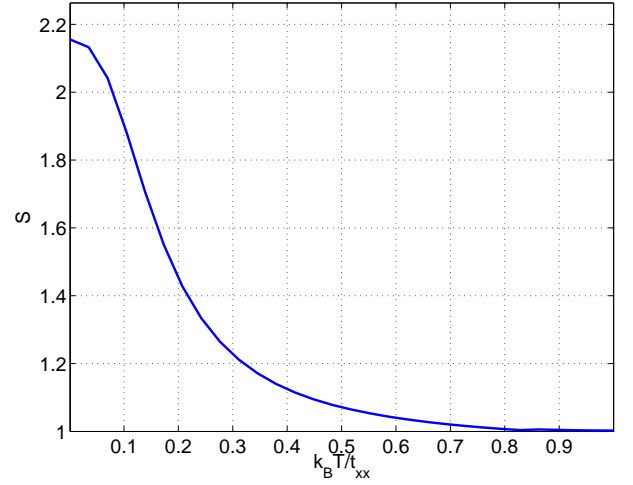


FIG. 2. (Color online) The anisotropy parameter  $S$  of the 2D density distribution as a function of the  $t_{xx}$ -scaled temperature for 1000 atoms, dimensionless trap strength  $\omega^2/2 = 0.001$  and potential depth  $V_x = V_y = 17$ .

and

$$H_{FD}^{(j)} = \frac{U_{xy} + U_{yx}}{2} |\psi_{xj}|^2 |\psi_{yj}|^2 \cos(2(\phi_{xj} - \phi_{yj})). \quad (34)$$

Here, the term accounting for the density-density interactions is phase independent and gives no information about the on-site phase ordering. However, the interflavor conversion term will explicitly depend on the phase difference between the  $x$ - and  $y$ -flavor order parameters, and accordingly, establishes an onsite interflavor phase locking. In fact, when  $U_{xy}, U_{yx} > 0$  the onsite energy is minimized with  $\phi_{xj} - \phi_{yj} = \pm\pi/2$ .

Now combining the above argument with the results of Sec. III, we obtain both the on- and inter-site full phase coherence of the condensate within the lattice. To this end we adopt the position representation of the onsite order parameter

$$\psi_j(\vec{r}) = \psi_{xj} w_{xj}(\vec{r}) + \psi_{yj} w_{yj}(\vec{r}) \quad (35)$$

and apply the requirements of phase locking, which yield

$$\psi_j(\vec{r}) = |\psi_{xj}| w_{xj}(\vec{r}) \pm i |\psi_{yj}| w_{yj}(\vec{r}), \quad (36)$$

where the  $\pm$ -sign alternates between neighboring sites. Note that in the absence of a trap, flipping the sign on all the sites gives a new configuration with exactly the same energy. This characteristic degeneracy, related to the swapping of the flavors  $x \leftrightarrow y$ , was already pointed out earlier. By furthermore considering the orthonormality property of Wannier functions,  $\int d\vec{r} w_{\alpha j}^*(\vec{r}) w_{\beta j}(\vec{r}) = \delta_{\alpha\beta} \delta_{jj}$ , we interpret the onsite order parameter as a spinor

$$\psi_j = \begin{bmatrix} |\psi_{xj}| \\ \pm i |\psi_{yj}| \end{bmatrix}, \quad (37)$$

where the spatial dependence has been absorbed into the basis states  $w_{xj}(\vec{r})$  and  $w_{yj}(\vec{r})$ . In particular, the length

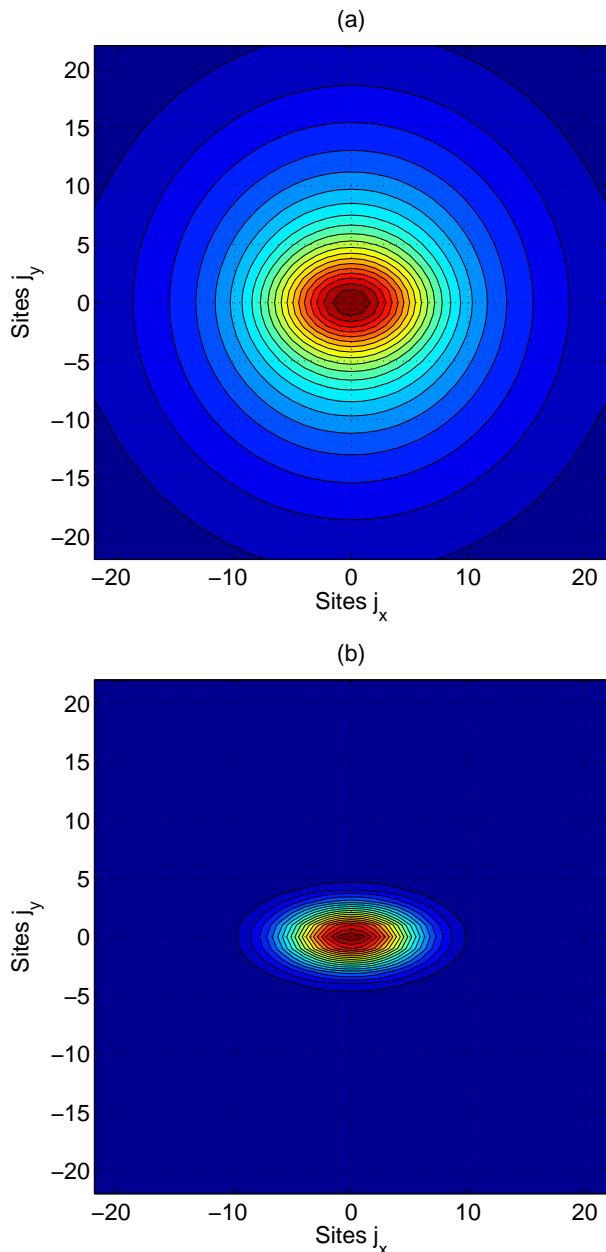


FIG. 3. (Color online) The populations per site (for a single atomic flavor) of the 2D Bose gas close ( $k_B T / t_{xx} = 1$ ) to the condensation critical temperature (a), and at  $T = 0$  (b). In both examples, the number of atoms is 1000, dimensionless trapping strength  $\omega^2/2 = 0.001$ , and potential depth  $V_x = V_y = 17$ .

of the spinor defined in this way gives the number of atoms at site  $\mathbf{j}$ , i.e.  $N_{\mathbf{j}} = \sqrt{|\psi_{x\mathbf{j}}|^2 + |\psi_{y\mathbf{j}}|^2}$ . For having the same properties as a two-level system, the spinor onsite order parameter can be fully characterized by the Bloch vector  $\mathbf{J}_{\mathbf{j}} = (J_{x\mathbf{j}}, J_{y\mathbf{j}}, J_{z\mathbf{j}})$ , where the components

are

$$\begin{aligned} J_{x\mathbf{j}} &= \psi_{x\mathbf{j}}^* \psi_{y\mathbf{j}} + \psi_{y\mathbf{j}}^* \psi_{x\mathbf{j}}, \\ J_{y\mathbf{j}} &= i \left( \psi_{x\mathbf{j}}^* \psi_{y\mathbf{j}} - \psi_{y\mathbf{j}}^* \psi_{x\mathbf{j}} \right), \\ J_{z\mathbf{j}} &= |\psi_{x\mathbf{j}}|^2 - |\psi_{y\mathbf{j}}|^2. \end{aligned} \quad (38)$$

In this picture, the length of the Bloch vector  $|\mathbf{J}_{\mathbf{j}}| = N_{\mathbf{j}}$  corresponds to the number of atoms at site  $\mathbf{j}$ ,  $J_{z\mathbf{j}}$  is the population imbalance between the two flavors, and due to the specific phase locking in (37), we have  $J_{x\mathbf{j}} = 0$ . We also point out that the Bloch vector constructed here corresponds to a mean-field version of the Schwinger angular momentum representation [30].

While the Bloch vector contains all the information about the spinor order parameter (37), it does not contain the full information on the spatial dependence of the onsite order parameter (36). This can be most easily investigated in the harmonic approximation, where the Wannier functions are replaced by harmonic eigenstates. Using this description, we have

$$\psi_{\mathbf{0}}^{(ha)}(\vec{r}) = [|\psi_{x\mathbf{0}}|x \pm i|\psi_{y\mathbf{0}}|y] e^{-\frac{x^2+y^2}{\sigma}} \quad (39)$$

with  $\sigma$  being the effective width determined from the lattice amplitude. It is clear that for  $|\psi_{x\mathbf{j}}| = |\psi_{y\mathbf{j}}|$  the above onsite order parameter represents a vortex/anti-vortex state with quantization  $L_{z\mathbf{j}}\psi_{\mathbf{j}}^{(ha)}(\vec{r}) = \pm\psi_{\mathbf{j}}^{(ha)}(\vec{r})$  where  $L_{z\mathbf{j}} = -i\partial_{\phi_{\mathbf{j}}}$ . This is only true, however, in the harmonic approximation and when  $J_{z\mathbf{j}} = 0$ . Beyond the harmonic approximation this is not strictly true even when  $J_{z\mathbf{j}} = 0$ . Nevertheless, due to the properties of the Wannier functions, Eq. (7), a  $\pi/2$  phase difference between flavors implies that the condensate density vanishes at the center of site  $\mathbf{j}$  and that the condensate has a vortex like singularity in it.

## B. Properties in the symmetric lattice

In the previous subsection we introduced the quantities characterizing the physical state within each site. For the global properties we use the anisotropy parameter as defined in Eq. (25). We numerically solve Eq. (19) by employing the split-operator method [31], which is based on factorization of the time-evolution operator into spatial and momentum parts. This implies that the method is exact only in the limit of vanishingly small time step. Therefore, propagation is divided into small time steps and we verify the numerical accuracy by varying their size. In order to find the ground state we propagate an initial trial state in imaginary time until convergence has been reached. It is generally seen that convergence is faster if we assume an initial guess with the phase ordering properties discussed in the previous section. It is also important to notice that a poor choice for the initial state may result in convergence to local, but not global,

energy minimum. To avoid this, we compare many different simulations where the initial trial state has been varied and the one with lowest final energy is assumed to be the ground state. The size of the grid is taken such that the atomic population is approximately zero at the edge of the grid, and in all simulations we consider a 2D system. The parameters of the Hamiltonian are calculated using the numerically obtained Wannier functions, and consequently we do not impose the harmonic approximation.

We have seen that the tunneling and the onsite interaction establish a phase locking according to Eq. (36). In a system without the external trap and  $U_0 \neq 0$ , it follows that  $J_{yj}/N_j$  will either be +1 or -1, and the system possesses a checkerboard structure, i.e. an anti-ferromagnet state with spins alternating between pointing in the positive or negative  $y$ -direction. The condensate will thus show the staggered vortex/anti-vortex structure. Within the validity of the tight-binding and single-band approximations, this result is exact. However, the strict vortex quantization  $L_{zj}\psi_j^{(ha)}(\vec{r}) = \pm\psi_j^{(ha)}(\vec{r})$  is only precise in the harmonic approximation. In the presence of the trap, the inhomogeneities in the density together with the tunneling anisotropy typically give rise to onsite interflavor population imbalance, which tends to break the anti-ferromagnetic order and lower the onsite angular momentum per particle from 1, which is expected from a quantized vortex with angular momentum along  $z$ .

The ground state lattice populations  $|\psi_{xj}|^2$  and  $|\psi_{yj}|^2$  for a system of  $V_x = V_y = 17$ ,  $\omega = 0.005$ , and  $U_0N = 1$  are displayed in Fig. 4 (a) and (b). It is clear how the anisotropy manifest itself, by rendering a condensate with spatially squeezed profile. In (c) we show the population imbalance  $J_{zj}$ . As we argued above, whenever  $J_{zj} \neq 0$  the anti-ferromagnetic order is broken, and from the figure it is evident that this is especially true in the edge of the condensate. To complement the results, we also present the corresponding Bloch vectors in Fig. 5 (a). Since  $J_{xj} = 0$ , it is enough to show the Bloch vector in the spin  $yz$ -plane  $\mathbf{J}_j = (0, J_{yj}, J_{zj})$ . By calling the horizontal axis the  $y$ -spin direction and the vertical axis the  $z$ -spin direction, we see that in the center of the condensate, the  $J_{yj}$  component dominates, while at the edge the Bloch vector no longer points along the horizontal direction demonstrating the breakdown of the anti-ferromagnetic order in these regions. Thus, at the center of the condensate where  $J_{zj} \approx 0$ , the anti-ferromagnetic ordering is still present.

In Fig. 6 we show the ground state lattice populations for a more strongly interacting system with  $U_0N = 15$ . In this case interactions and trap energies are larger than the kinetic energy and we approach the TF regime. We can see how the effects of the anisotropic density are now smoothed and the region of the center of the trap is enlarged. The latter also corresponds to the region where non-trapped like physics actually occurs, as confirmed in Fig.5 (b), by the presence of almost horizontal Bloch vectors. This also implies that now the ferromagnetic order extends over more sites in the lattice.

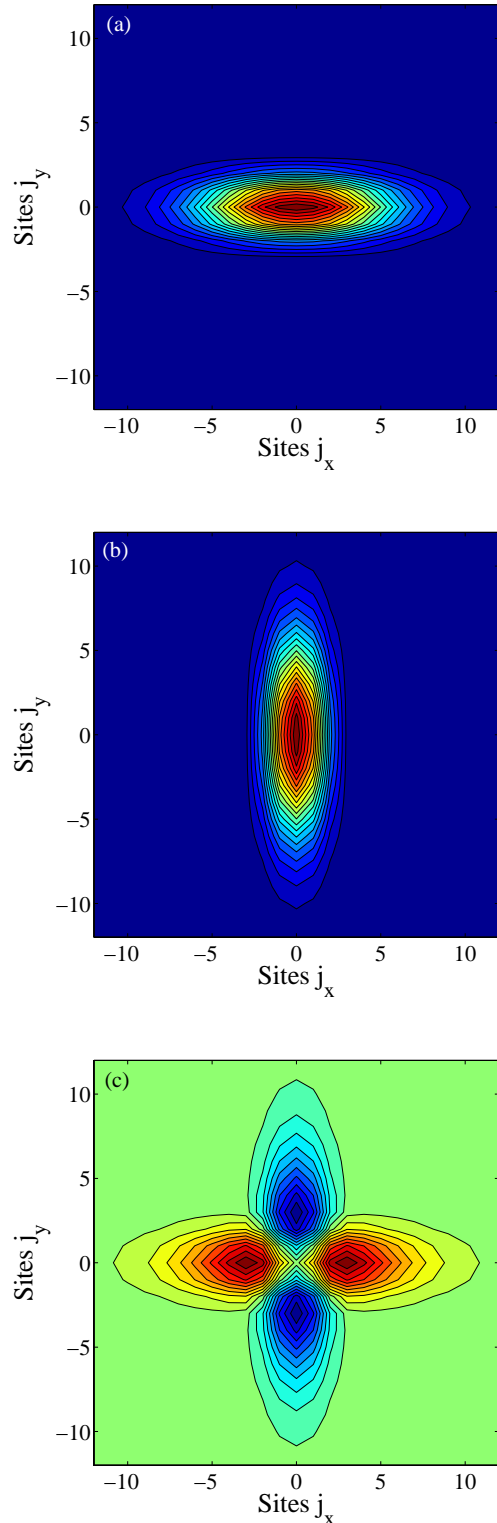


FIG. 4. (Color online) Upper two plots (a) and (b) show the  $x$ - and  $y$ -flavor ground state population respectively. The lower plot (c) gives instead the corresponding population imbalance  $J_{zj}$ . The dimensionless system parameters are  $V_x = V_y = 17$ ,  $\omega = 0.005$ , and  $U_0N = 1$ . (Red color indicates an excess of  $x$ -flavor atoms while blue regions have an excess of  $y$ -flavor atoms.)

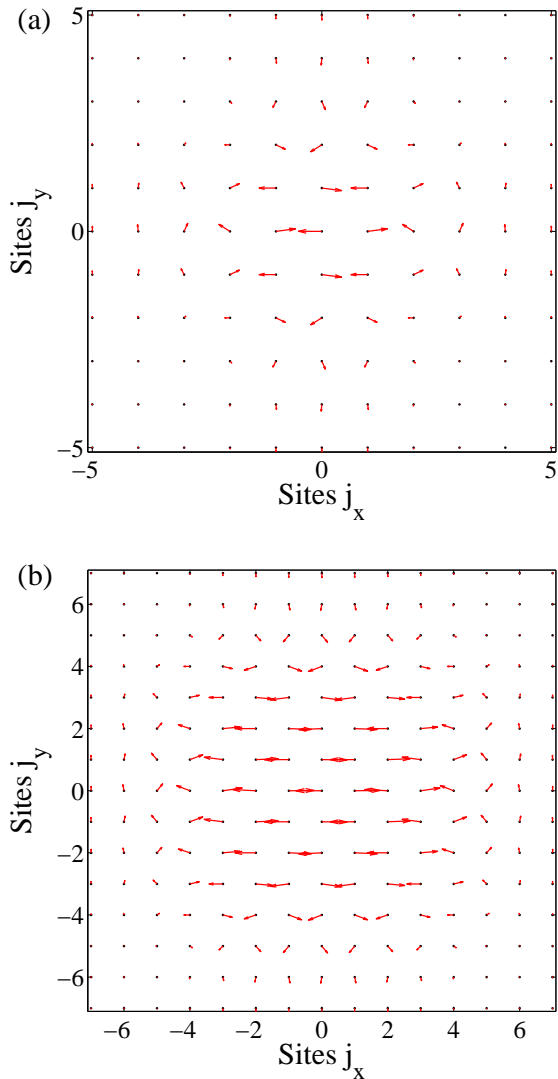


FIG. 5. (Color online) The Bloch vector at the different lattice sites (the  $x$ -component is strictly zero). The  $y$ -spin direction has been chosen along the horizontal axis and the  $z$ -spin direction along the vertical axis. The length of the vector represents the density, while the offset from the horizontal axis indicates breakdown of the anti-ferromagnetic order. The lattice sites are marked by black dots. The upper plot (a) gives the results where interaction plays a minor role,  $U_0 N = 1$ , while in (b)  $U_0 N = 15$  and interaction cannot be ignored. The rest of the parameters are the same as for Fig. 4.

We complete the study of the interacting system's ground state in the symmetric lattice by investigating the behavior of the anisotropy parameter (25). Here, the relevant question to be understood is related to characterization of  $S$  when the system undergoes a transition to the TF regime. When the kinetic energy becomes suppressed, the anisotropy should vanish and hence  $S \rightarrow 1$ . In the lattice there are two ways of suppressing the kinetic energy, either by increasing the interparticle inter-

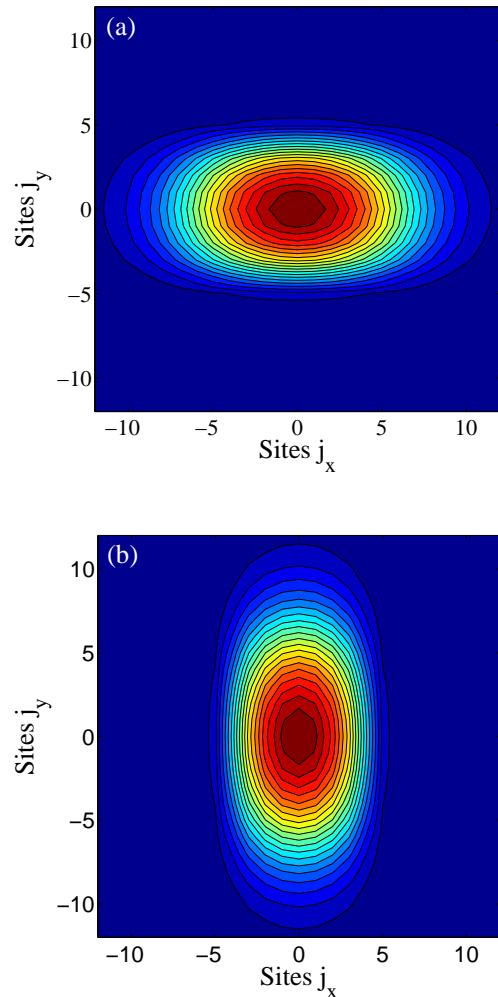


FIG. 6. (Color online) Plots showing the  $x$ - (a) and  $y$ -flavor (b) ground state populations, respectively, for the dimensionless system parameters  $V_x = V_y = 17$ ,  $\omega = 0.005$ , and  $U_0 N = 15$ . Due to the larger interaction, the squeezing effect is not as pronounced in this case compared to Fig. 4.

action strength  $U_0$  directly by making use of Feshbach resonances, or by considering larger potential amplitudes. The predicted behavior of  $S$  is shown in Fig. 7. Note, that increasing  $U_0 N$  leads to a monotonic decrease of  $S$  until it asymptotically reaches 1. In the other case, where variation of  $V = V_x = V_y$  is considered,  $S$  also approaches 1 asymptotically, but now the behavior is not monotonic. This anomalous and surprising behavior does not appear in the continuum approximation. It should be noted that the continuum limit is evaluated in the ideal limit of  $U_0 = 0$ , and we especially have that  $S_{con}$  is not approaching 1 as  $V \rightarrow \infty$ . In this limit, on the other hand, any small  $U_0 > 0$  will imply  $S = 1$  since the kinetic term is negligible compared to the interactions. For small and moderate  $V$ , the continuum result (26) is found to increase monotonously for increasing val-

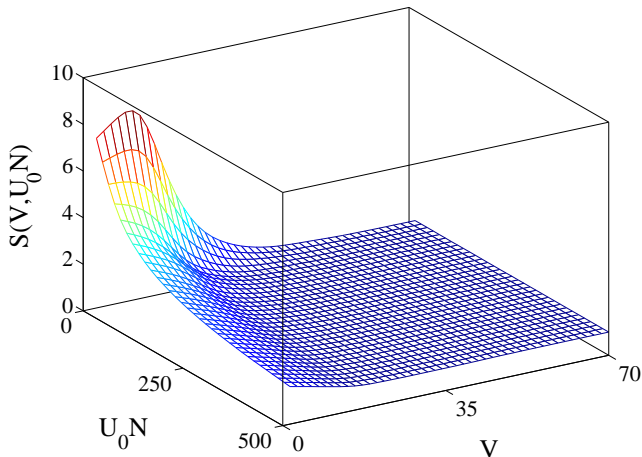


FIG. 7. (Color online) The condensate anisotropy parameter  $S$  as defined in Eq. (25) as a function of the interaction strength  $U_0 N$  and the lattice amplitude  $V = V_x = V_y$ . Whenever the amplitude or the interaction become large, the squeezing approaches one and the condensate enter into the TF regime. The dimensionless trap frequency  $\omega = 0.005$ .

ues of  $V$ . This behavior is not found for the discrete model, even for  $U_0 = 0$ . Thus, for large amplitudes the discrete and continuum models predict qualitatively different results for the squeezed profile of condensate in terms of the anisotropy parameter. We should also point out that for small amplitudes, typically  $V < 5E_r$  [26], the tight-binding approximations break down and the results should not be taken too literally in this regime.

### C. Properties in the anisotropic lattice

Asymmetry in the lattice breaks the degeneracy of  $x$  and  $y$  flavors. In order to investigate the effect of anisotropies we introduce the asymmetry parameter

$$R = \frac{V_x}{V_y} \quad (40)$$

which controls the ratio between the lattice depths, such that  $R = 1$  represents the symmetric lattice configuration we discussed earlier. We have numerically verified that the dominant effect of the asymmetry is to shift the energy levels of  $x$ - and  $y$ -flavors. By considering only a single site first, we note that in the harmonic approximation this shift equals

$$\Delta = E_y - E_x = 2\sqrt{V_x}(\sqrt{R} - 1), \quad (41)$$

where  $E_x$  and  $E_y$  are the energies of the onsite flavors, i.e.  $E_\alpha = \int d\vec{r} w_{\alpha\mathbf{j}}^*(\vec{j}) [-\nabla + V_{latt}(\vec{r})] w_{\alpha\mathbf{j}}(\vec{j})$  and where the  $\mathbf{j}$  dependence vanishes. In this single site picture, this splitting will have only a small effect if it is much

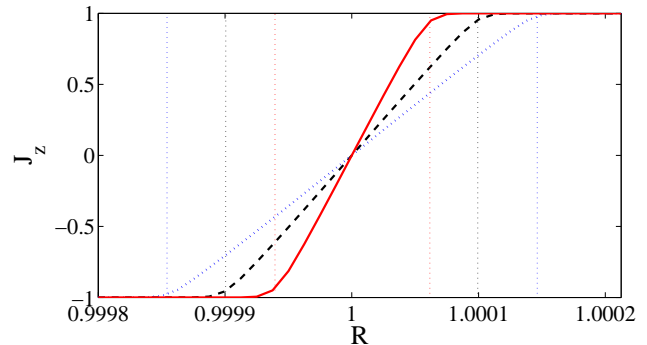


FIG. 8. (Color online) The parameter  $J_z$  as a function of the lattice asymmetry parameter  $R$ , for three different trapping frequencies,  $\omega = 0.003$  (red solid line),  $\omega = 0.005$  (black dashed line), and  $\omega = 0.007$  (blue dotted line). The vertical dashed thin lines indicate the typical sizes of  $\delta$  which determines the transition region where the two atomic flavors co-exist. It is clear how  $\delta$  is decreased when the trap is “opened up” (decreasing  $\omega$ ). The remaining dimensionless parameters are  $U_0 N = 1$  and  $V_x = 17$  (meaning that  $V_y = 17/R$ ).

smaller than the characteristic interaction energy scale  $E_{int} \sim U_0 N |\psi_x|^2$ .

The picture becomes more complicated when we consider more sites. It can be, for example, that the region  $\delta$  around  $R = 1$  in which interaction mixes the two flavors changes as the trapping strength is varied, and in particular, if  $\delta$  is small, the properties of the ground state may change dramatically with small variations in the various lattice parameters. On the other hand, if these parameters can be controlled, the physics around the degeneracy point might lead to novel physics similar to the adiabatic driving considered recently in Ref. [32]. However, it is worth pointing out that the present model possesses an additional property, namely that the  $x$ - and  $y$ -flavor densities are spatially different and adiabatic driving between the two might therefore lead to macroscopic particle flow within the trap. While interesting, this time-dependent aspect will be addressed elsewhere.

The asymmetries for our square lattice can in principle be implemented in two ways, either by considering a lattice with different wave vectors  $k_x$  and  $k_y$  or different amplitudes  $V_x$  and  $V_y$ . Here we characterize the behavior of the system in the latter process. The sensitivity to  $R$  can be analyzed, for example, in the value of the mean population inversion

$$J_z = \frac{1}{N} \sum_{\mathbf{j}} J_{z\mathbf{j}}. \quad (42)$$

If  $J_z = -1$ , the system consists of only  $y$ -flavor atoms, and  $J_z = +1$  represents only atoms in the  $x$ -flavor. Thus,  $J_z$  gives a measure of how much interaction mixes the two flavors. In the vicinity of  $R = 1$ , the properties of  $J_z$  are illustrated in Fig. (8). It clearly shows uniquely occupied flavors in both regions where  $R < 1$  and  $R > 1$ . Also, as

expected, the exact point  $R = 1$  is characterized by equal sharing of population among the two flavors, and therefore one recovers the properties of the degenerate system. As pointed out above, the non-zero interaction ( $U_0 \neq 0$ ) is crucial in order to stabilize the equal population at  $R = 1$ .

The confinement imposed by the harmonic trap implies that we are dealing with a finite size system. The frequency  $\omega$  sets, in some sense, the system size and, as we discussed above, it is interesting to understand how  $\delta$  depends on the system size. Figure (8) depicts the variations of  $J_z$  around  $R = 1$ , and it is seen how these become more dramatic when  $\omega$  is decreased. More precisely, there seems to be a one-to-one correspondence between the range  $\delta$  in which  $|J_z| < 1$  and  $\omega$ , and as  $\omega \rightarrow 0$  the plot indicates also that  $\delta \rightarrow 0$ . This suggests (for very weakly interacting systems) similar behavior to the one generally exhibited by systems undergoing a first order phase transition [33]. In addition, we also studied the ground state energy  $E_0(R)$  and found that  $dE_0(R)/dR$  shows a pronounced change around  $R = 1$  as  $\omega$  is decreased. We have also numerically verified that the range  $\delta$  grows for increasing interaction strength  $U_0N$  in agreement with our earlier argument that interaction mixes the flavors.

The above findings suggest that for weak interactions a careful adjustment of the lattice is required in order to study the anti-ferromagnetic properties. As interactions become stronger the anti-ferromagnetic properties become more robust. In experimental realizations even a small temperature might actually help to establish a phase coherence between  $x$ - and  $y$ -flavor atoms since the energy gap between the ground and first excited energies greatly decreases around the  $R = 1$  point and in its vicinity one may expect population also of the first excited state. We furthermore notice that for non-zero  $\omega$ , the transition from one to the other extreme of  $J_z$  is smooth, and therefore by controlling the lattice amplitudes the system could be considered for studies of the many-body Landau-Zener transition [34] or the Kibble-Zurek mechanism [35].

## V. CONCLUSION

We have investigated how a confining potential affects the properties of bosonic atoms residing on the  $p$ -bands of optical lattices. Our focus was on the 2D square lattice with equal lattice amplitudes in the two directions and we restricted our analysis to a mean-field approach. It is known that for a  $p$ -band square lattice model, even at a mean-field level the ground state forms non-trivial states in terms of an anti-ferromagnetic order [5, 9]. As a result of the anisotropic tunneling on the  $p$ -band together with the confinement introduced by the trap, we showed that the anti-ferromagnetic structure is destroyed in the edges of the condensate. The effects of the tunneling anisotropy are also manifest in the density profile of the atomic cloud, yielding a spatially elongated condensate

in one of the two spatial directions, despite the isotropic trap. We showed how this narrowing is suppressed when the kinetic energy is lowered, either due to increasing of the strength of atom-atom interactions and/or due to increasing the lattice amplitudes. The same suppression was found also for the ideal gas when the temperature is increased and thereby the properties of the gas are greatly determined by thermal atoms. By considering unequal lattice amplitudes in the  $x$ - and  $y$ -directions, the degeneracy on the  $p$ -bands is broken, and we demonstrated that the sensitivity of the ground state properties depend strongly on the system “size”. The results presented are for 2D lattices, but it is understood that the general findings directly generalize to 3D as well. In the 3D cubic case, the phase ordering can be more complicated [9], but as in the 2D case, this ordering would also be destroyed in the edges of the condensate in a trapped system.

One point we have not addressed concerns experimental realizations. The main source for dissipation and decoherence in the square lattices is scattering of two  $p$ -band atoms into one  $s$ - and one  $d$ -band atom [9, 23]. This process is resonant in the harmonic approximation, while it is generally off-resonant for actual lattices, which causes the typical life-time for  $p$ -band atoms to be much larger than the characteristic tunneling times. In Ref. [23], coherence of  $p$ -band atoms in a cubic lattice was indeed demonstrated. Alternatives for suppressing this decay further include loading fermionic atoms into the  $s$ -band of the lattice [36] or considering experimental setups with non-separable lattices [19, 20, 37]. In the first case, the presence of fermions in the  $s$ -band prevents the bosonic  $p$ -band atoms to occupy the lowest band due to atom-atom interactions. Now in configurations involving non-separable lattices (e. g. superlattices), few bands can be separated from the rest, and thus the role of the ( $p + p \rightarrow s + d$ ) scattering becomes overshadowed. In Refs. [19, 20], however, the experimental setup gives rise to hybridization of different flavor atoms and the analysis becomes more complex than the one for the simple square lattice considered here.

Another important experimentally relevant question concerns detection of the presented predictions. If the detection makes no difference between  $x$ - and  $y$ -flavor atoms, the Bloch vector cannot be fully measured. However, in a recent work it was suggested how such measurements can indeed be performed [38]. The idea utilizes Raman pulses that rotate the spinor (37) similar to qubit measurements in atomic physics [39]. Moreover, in a recent experiment on triangular lattices [27] it was demonstrated how the phase of the condensate affects the densities in time-of-flight measurements. We have numerically studied the full condensate order parameter  $\Psi(x, y)$ , and found that coherence within single sites are seen in  $\Psi(x, y)$  while long range coherence is manifested in the momentum distribution of  $\Psi(x, y)$ . This means that if the condensate density  $|\Psi(x, y)|^2$  is detected at different time instants in a time-of-flight measurements,

one could in principle extract all information about the phase coherence.

We believe that entering the more strongly correlated regime where quantum fluctuations become more important would be of interest. The mean-field method adopted here is not capable of capturing these effects, and we therefore leave this investigation for the future. We especially intend to study the “wedding cake” structure [25] formed by alternating insulating Mott and superfluids in the presence of a harmonic trap, as well as non-equilibrium properties of the system.

## ACKNOWLEDGMENTS

Financial support from the Swedish Research Council (Vetenskapsrådet) is acknowledged. JL acknowledges financial support from DAAD (Deutscher Akademischer Austausch Dienst) and the Royal Research Council Sweden (KVA). JPM acknowledges financial support from the Academy of Finland (Project 135646).

- 
- [1] I. Bloch, J. Dalibard, and W. Zwerger, *Rev. Mod. Phys.* **80**, 885 (2008).
- [2] M. Lewenstein, A. Sanpera, V. Ahufinger, B. Damski, A. Sen(De), and U. Sen, *Adv. Phys.* **56**, 243 (2007).
- [3] M. Greiner, O. Mandel, T. Esslinger, T. W. Hänsch, and I. Bloch, *Nature* **415**, 39 (2002).
- [4] M. Lewenstein and W. V. Liu, *Nature Phys.* **7**, 101 (2011).
- [5] A. Isacsson and S. M. Girvin, *Phys. Rev. A* **72**, 053604 (2005).
- [6] V. W. Scarola and S. Das Sarma, *Phys. Rev. Lett.* **95**, 033003 (2005); V. W. Scarola, E. Demler, and S. Das Sarma, *Phys. Rev. A* **73**, 051601 (2006).
- [7] C. J. Wu, W. V. Liu, J. Moore, and S. Das Sarma, *Phys. Rev. Lett.* **97**, 190406 (2006).
- [8] C. Xu and M. P. A. Fisher, *Phys. Rev. B* **75**, 104428 (2007).
- [9] A. Collin, J. Larson, and J.-P. Martikainen, *Phys. Rev. A* **81**, 023605 (2010).
- [10] O. E. Alon, A. I. Streltsov, and L. S. Cederbaum, *Phys. Rev. Lett.* **95**, 030405 (2005).
- [11] J. Larson, A. Collin, and J.-P. Martikainen, *Phys. Rev. A* **79**, 033603 (2009).
- [12] K. R. A. Hazzard and E. J. Mueller, *Phys. Rev. A* **81**, 031602(R) (2010).
- [13] X. Li, E. Zhao, W. V. Liu, *Phys. Rev. A* **83**, 063626 (2011); D.-S. Luehmann, O. Juergensen, and K. Sengstock, arXiv:1108.3013; U. Bissbort, F. Deuretzbacher, and W. Hofstetter, arXiv:1108.6047.
- [14] H. P. Büchler, *Phys. Rev. Lett.* **104**, 090402 (2010); J. von Stecher, V. Gurarie, L. Radzihovsky, and A. M. Rey, *Phys. Rev. Lett.* **106**, 235301 (2011).
- [15] T. Busch, B.-G. Englert, K. Rzazewski, and M. Wilkens, *Found. Phys.* **28**, 549 (1998).
- [16] G. K. Campbell, J. Mun, M. Boyd, P. Medley, A. E. Leanhardt, L. G. Marcassa, D. E. Pritchard, and W. Ketterle, *Science* **313**, 649 (2006).
- [17] S. Will, T. Best, U. Schneider, L. Hackermüller, D.-S. Lühmann, and I. Bloch, *Nature* **465**, 197 (2010).
- [18] P. R. Johnson, E. Tiesinga, J. V. Porto, and C. J. Williams, *New J. Phys.* **11** 093022 (2009).
- [19] G. Wirth, M. Ölschläger, and A. Hemmerich, *Nature Phys.* **7**, 147 (2011).
- [20] M. Ölschläger, G. Wirth, and A. Hemmerich, *Phys. Rev. Lett.* **106**, 015302 (2011).
- [21] W. V. Liu and C. Wu, *Phys. Rev. A* **74**, 013607 (2006); C. Wu, *Mod. Phys. Lett.* **23**, 1 (2009).
- [22] J. H. Denschlag, J. E. Simsarin, H. Häffner, C. McKenzie, A. Browaeys, D. Cho, K. Helmerson, S. L. Rolston, and W. D. Phillips, *J. Phys. B* **35**, 3095 (2002); A. Browaeys, H. Häffner, C. McKenzie, S. L. Rolston, K. Helmerson, and W. D. Phillips, *Phys. Rev. A* **72**, 053605 (2005).
- [23] T. Müller, S. Fölling, A. Widera, and I. Bloch, *Phys. Rev. Lett.* **99**, 200405 (2007).
- [24] C. Wu, W. V. Liu, J. Moore, and S. Das Sarma, *Phys. Rev. Lett.* **97**, 190406 (2006); C. Wu, D. Bergman, L. Balents, and S. Das Sarma, *Phys. Rev. Lett.* **99**, 070401 (2007); C. Wu, *Phys. Rev. Lett.* **100**, 200406 (2008).
- [25] K. Mitra, C. J. Williams, and C. A. R. Sa de Melo, *Phys. Rev. A* **77**, 033607 (2008).
- [26] D. van Oosten, P. van der Straten, and H. T.C. Stoof, *Phys. Rev. A* **63**, 053601 (2001); J. Larson, S. Fernandez-Vidal, G. Morigi, and M. Lewenstein, *New J. Phys.* **10**, 045002 (2008).
- [27] J. Struck, C. Ölschläger, R. Le. Target, P. Soltan-Panahi, A. Eckardt, M. Lewenstein, P. Windpassinger, and K. Sengstock, *Science* **333**, 996 (2011).
- [28] M. Aunola, *J. Math. Phys.* **44**, 1913 (2003).
- [29] C. J. Pethick and H. Smith, *Bose-Einstein Condensation in Dilute Gases*, (Cambridge University Press, Cambridge, 2008).
- [30] J. J. Sakurai, *Modern Quantum Mechanics*, (Addison Wesley, 1995).
- [31] M. D. Fleit, J. A. Fleck, and A. Steiger, *J. Comput. Phys.* **47**, 412 (1982).
- [32] M. Ölschläger, G. Wirth, T. Kock, and A. Hemmerich, *Phys. Rev. Lett.* **108**, 075302 (2012).
- [33] S. Sachdev, *Quantum Phase Transitions*, (Cambridge University Press, Cambridge, 1997).
- [34] A. Altland, V. Gurarie, T. Kriecherbauer, and A. Polkovnikov, *Phys. Rev. A* **79**, 042703 (2009); A. P. Itin and P. Törmä, *Phys. Rev. A* **79**, 055602 (2009); Y.-A. Chen, S. D. Huber, S. Trotzky, I. Bloch, and E. Altman, *Nature Phys.* **7**, 61 (2011).
- [35] T. W. B. Kibble, *J. Phys. A* **9**, 1387 (1976); W. H. Zurek, *Nature* **317**, 505 (1985).
- [36] W. V. Liu and C. Wu, *Phys. Rev. A* **74**, 013607 (2006).
- [37] M. Foss-Feig and A. M. Rey, *Phys. Rev. A* **84**, 053619 (2011).
- [38] Z. Cai, L.-M. Duan, and C. Wu, arXiv:1110.3021.
- [39] S. Haroche and J.-M. Raimond, *Exploring the Quantum*, (Oxford University Press, Oxford, 2006).